ELSEVIER

Structure and dielectric characterization of a new A-site deficient $La_{5/3}MgTaO_6$ perovskite

D.D. Khalyavin[a,*], A.M.R. Senos[a], P.Q. Mantas[a], D.N. Argyriou[b], I. Tarroso Gomes[c], L.G. Vieira[c], J.L. Ribeiro[c]

[a]Department of Ceramics and Glass Engineering, CICECO, University of Aveiro, Aveiro 3810-193, Portugal
[b]Hahn-Meitner-Institut, Glienicker Straße 100, Berlin D-14109, Germany
[c]Department of Physics, University of Minho, Braga 4710-057, Portugal

Abstract

The crystal structure of new A-site deficient $La_{5/3}MgTaO_6$ perovskite was investigated by neutron, X-ray and electron diffraction. Neutron and X-ray powder diffraction spectra were refined in the monoclinic $I2/m$ space group, with the parameters of the unit cell $a = 5.6304(2)$ Å, $b = 5.6226(2)$ Å, $c = 7.9434(2)$ Å and $\beta = 90.04(1)°$. This structural model presumes a random distribution of the vacancies and takes into account both a rock salt-type Mg^{2+}/Ta^{5+} cation ordering and $a^- a^- c^0$ configuration of the octahedral tilting. Electron diffraction showed that the crystal structure is more complex at the local level due to a short-range vacancy ordering. This observation in combination with the symmetry analysis leads to the conclusion that the $C2/m$ symmetry with $2\sqrt{2}a_p \times 2\sqrt{2}a_p \times 2a_p$ supercell is more adequate for the description of the crystal structure in the local level. Dielectric measurements performed in a wide frequency range were correlated with the crystal structure and compared with other ordered double perovskites. Far-infrared spectroscopy was used to characterize the lattice contribution to the dielectric response at the microwave frequencies. The complex dielectric function was evaluated and extrapolated down to the gigahertz range. The effect of the vacancies on the intrinsic dielectric losses is discussed based on the spatial phonon correlation model.
© 2006 Elsevier Inc. All rights reserved.

Keywords: A-site deficient perovskite; Octahedral tilting; Dielectric properties; Neutron diffraction; Infrared spectroscopy; Phonon correlation model

1. Introduction

Due to the flexibility of the perovskite structure to incorporate a considerable amount of vacancies, a relatively large number of new anion or cation deficient perovskites are being designed. The possible formation of superstructures arising from the ordering of the vacancies is of particular interest, because these materials do often exhibit useful and interesting properties. For example, A-site deficient perovskites, $Ln_{2/3}TiO_3$ and $Ln_{1/3}Nb/TaO_3$ (Ln-lanthanide), are used in components for microwave application [1,2] and those doped with alkaline metals are used in ion-conducting solid electrolytes [3–5]. The anion-deficient perovskites $LnBa_2Cu_3O_{7+\delta}$ and $LnBaCo_2O_{5+\delta}$

exhibit high-temperature superconductivity [6,7] and giant magnetoresistance [8,9] phenomena, respectively. In the first example, the ordering of the vacancies in the A-site position results in a layer type of the crystal structure, with an interchange between the (0 0 1) planes containing only vacancies or lanthanide ions and mixed planes statistically populated by vacancies and ions.

Recent structural investigations [10,11] have revealed that additional ordering of the vacancies in the mixed planes could be induced by the presence of cation ordering in the B-site position. The layered oxides $La_4Mg_3W_3O_{18}$ and $La_6Mg_4Ta_2W_2O_{24}$, with rock-salt type ordering between Mg^{2+} and W^{6+}/Ta^{5+}, exhibit an interchange between the fully and the partially occupied lanthanum layers, with a row-type vacancy ordering in the lanthanum poor layers. Based on the superstructures observed in these perovskites, a new homologous series, $A_{3n}B'_{2n}B''_{2n}O_{12n}$,

*Corresponding author. Fax: +351 234 425 300.
E-mail address: dkhalyavin@cv.ua.pt (D.D. Khalyavin).

was identified [11]. $La_4Mg_3W_3O_{18}$ and $La_6Mg_4Ta_2W_2O_{24}$ are representatives of the $n = 1$ and 2 families, respectively. The strategy to obtain new members of the series, with a higher n value, is to decrease both the charge difference between B' and B'' cations and the concentration of vacancies in the lanthanum poor layers. Therefore, the initial aim of the present work was to obtain a new member of the homologous series with a higher n value. The $La_{5/6}Mg_{1/2}Ta_{1/2}O_3$ ($La_{5/3}MgTaO_6$) composition was chosen for this reason. By combining X-ray, neutron and electron diffractions, it was found that a single perovskite phase is formed in this composition, but a vacancy ordering is only observed in a short-range scale.

The nearly statistical distribution of the vacancies makes this compound interesting to study the effect of the cation vacancies on the electrical properties, particularly on the dielectric loss. Therefore, dielectric measurements in a wide frequency range were carried out and the role of the cation vacancies in the mechanism of absorption of electromagnetic waves in the gigahertz range is discussed.

2. Experimental

To prepare the $La_{5/3}MgTaO_6$ oxide, powders of La_2O_3 (99.5%, Merck), MgO (98%, Fluka) and Ta_2O_5 (99.9%, Riedel-de Haën) were weighed according to the stoichiometry of the composition and mixed for 4 h in a polyethylene container with ethanol and zirconia balls, in a planetary mill. The slurries were dried in an oven at 120 °C and the dried powders were deagglomerated. The powders were then calcined at 1200 °C for 4 h. After calcination, the materials were deagglomerated again. Finally, pellets with 10 mm diameter and 5–6 mm height were obtained by uniaxial pressing in a steel die under 60 MPa, followed by an isostatic pressing at 200 MPa. The pellets were sintered in air for 6 h at 1500 °C. The heating and cooling rates were 360 °C/h. Weight losses during the sintering did not exceed 1.5%. The microstructure and the cation composition of the sintered specimens were characterized by scanning electron microscopy (SEM) and energy dispersive spectroscopy (EDS), respectively, using a Hitachi S-4100 microscope equipped with a Rontec spectrometer.

To obtain powders for neutron and X-ray diffraction experiments, the sintered pellets were crushed in an agate mortar. The room temperature powder neutron diffraction pattern was recorded on the fine resolution powder diffractometer (FIREPOD) of the Berlin Neutron Scattering Center (BENSC) with incident neutrons of wavelength $\lambda = 1.7974$ Å [(511) reflection of a vertically bent Ge monochromator] and collimation $\alpha_1 = 18'$ (in pile collimator), $\alpha_2 = 20'$ (second collimator after the monochromator), $\alpha_3 = 10'$ (third collimator after the sample). Data were collected in the angular range of $0° < 2\theta < 160°$. X-ray powder diffraction data were obtained using a Rigaku D/MAX-B diffractometer (CuKα radiation; tube power 40 kV, 30 mA; 2θ range 0–120°, step 0.02°, 10 s/step;

graphite monochromator; receiving slit 0.15 mm). The obtained data were refined by the Rietveld method using the Fullprof suite [12].

Ceramics samples used for the transmission electron microscopy (TEM) observations were ground to about 30 μm and then milled until perforation using a BAL-TEC Ion Mill (RES 100). The samples were examined using a Hitachi H9000-NA TEM, operating at 300 kV.

Samples for the radio frequency dielectric measurements were polished to form disks with a thickness of 0.4–0.5 mm, electroded with platinum paste and annealed at 1000 K. Dielectric response was measured as a function of temperature, in the frequency range of $10^2–10^6$ Hz, using a Precision LCR meter (HP 4284A). Measurements were performed over the interval 300–950 K at cooling with a rate of 1 K min^{-1}. The room temperature permittivity, Q-factor ($Q = 1/\tan\delta$) and resonant frequency, f, of the samples in the microwave frequency range were estimated by an adaptation of the Hakki-Coleman method [13,14] using a 10 MHz—20 GHz Scalar Analyser (IFR 6823).

Far-infrared (FIR) reflectivity measurements were performed with a Brüker IFS-66 V spectrometer in the spectral range of 40–4000 cm^{-1}. Room temperature pyroelectric detectors of DTGS with PE or KBr windows and 6 μM8 Mylar or KBr beam-splitters were used in the FIR and medium IR ranges, respectively. The IR complex dielectric permittivity was evaluated by fitting the spectra to the factorized form of the dielectric function, with equal LO and TO damping coefficients. Under such condition, this factorized form is equivalent to the usual sum of Lorentz oscillators.

3. Results and discussion

3.1. Crystal structure

The room temperature X-ray diffraction pattern of $La_{5/3}MgTaO_6$ is presented in Fig. 1. In a first approximation it can be indexed in a cubic unit cell, with $a–2a_p$ (a_p is the parameter of the pseudocubic perovskite subcell). The reflection conditions are consistent with the face centred $Fm\bar{3}m$ space group, which is a characteristic of the undistorted rock-salt type ordered $A_2B'B''X_6$ perovskites. No additional reflections, which could be associated to the A-site cation ordering, is observed. The examination of the high-angle fundamental reflections revealed that these peaks are slightly broadened (Fig. 1 inset) ruling out cubic symmetry. Distortions of the perovskite structure are often observed and the most probable case is that of oxygen atoms displacements (octahedral tilting). To study this possibility in the present case, a high-resolution neutron powder diffraction experiment was performed. As expected, the agreement between the observed and the calculated in the $Fm\bar{3}m$ space group patterns was poor (Table 1) and, therefore, lower symmetry space groups were tested. The selection of the model was based on the results of the group theoretical analysis performed by
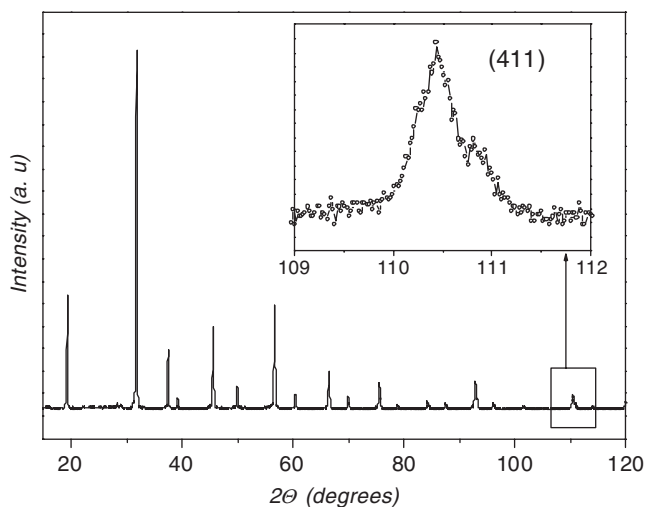
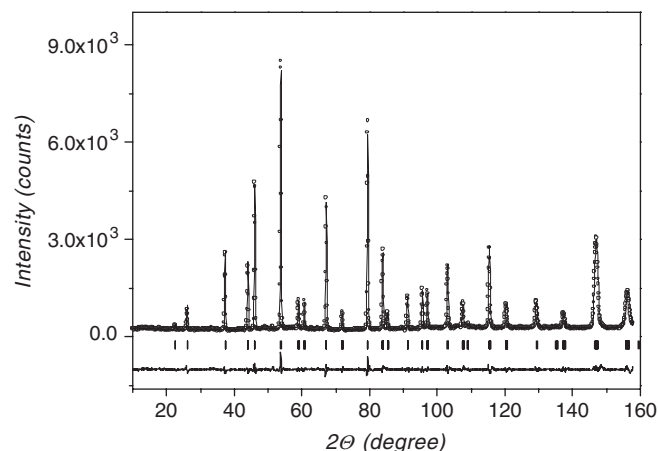Fig. 1. X-ray diffraction pattern of $La_{5/3}MgTaO_6$. The inset shows the (411) fundamental multiplet.

Fig. 2. Observed (circles), calculated (continuous curve) and difference (solid line below the spectrum) neutron diffraction pattern ($\lambda = 1.7974$ Å) of $La_{5/3}MgTaO_6$.

Table 1
Reliability factors obtained in the refinement of the high resolution neutron diffraction data for $La_{5/3}MgTaO_6$, using different models with isotropic thermal parameters

Space group	R_p (%)	R_{wp} (%)	R_{Bragg} (%)	χ^2
$Fm\bar{3}m$	22.6	34.0	44.5	49.2
$I4/m$	8.8	11.9	11.3	6.07
$R\bar{3}$	8.0	10.9	9.0	5.09
$I2/m$	6.0	7.8	4.0	2.61
$I\bar{1}$[a]	—	—	—	—

[a]Refinement was unstable in this space group and a convergence was not reached.

Howard et al. [15] for octahedral tilting in the $A_2B'B''X_6$ double perovskites. Taking into account the absence of the $\{hkl;\ h,\ k=2n+1,\ k=2n\}$ reflections (in the $2a_p \times 2a_p \times 2a_p$ unit cell indexation), which are associated with in-phase octahedral tilting, four space groups, $I4/m$, $R\bar{3}$, $I2/m$ and $I\bar{1}$ compatible with the antiphase rotation of the octahedra, $a^0a^0c^-$, $a^-a^-a^-$, $a^-a^-c^0$ and $a^-b^-c^-$ tilt systems, respectively, were considered. The final conclusion based on a comparison of the corresponding reliability factors (Table 1) favoured the monoclinic $I2/m$ space group ($C2/m$ in standard setting). The refined spectrum using this model is shown in Fig. 2 and a schematic representation of the crystal structure is shown in Fig. 3. The obtained structural parameters are summarized in Tables 2 and 3.

The data demonstrate that the nearly regular octahedra, with metal-oxygen bond distances being 2.06 Å and 1.97 Å for magnesium and tantalum, respectively, are tilted in the $a^-a^-c^0$ configuration, with an angle of rotation about the [100] and [010] pseudocubic axes of $\sim 7^\circ$. The refinement was performed on the assumption of fully occupied $2a$ and $2d$ positions by magnesium and tantalum, respectively. The obtained coordinates were then used to refine the X-ray diffraction pattern. In this refinement procedure, the B-site
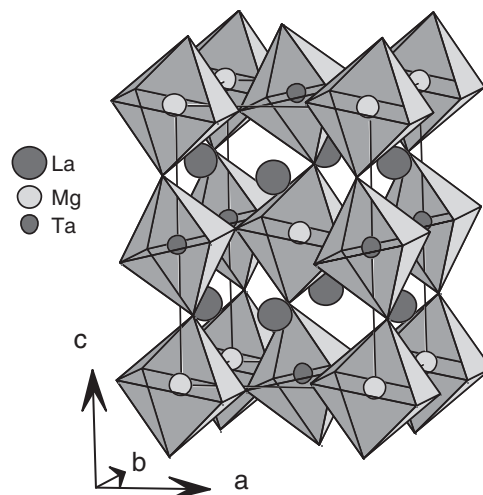

Fig. 3. Schematic representation of the crystal structure of $La_{5/3}MgTaO_6$ ($I2/m$ symmetry, $\sqrt{2}a_p \times \sqrt{2}a_p \times 2a_p$ unit cell). 83% of the lanthanum position is occupied.

cation occupancies were allowed to vary. However, it did not reveal any $2a \leftrightarrow 2d$ anti-site substitutions.

The chemical composition of $La_{5/3}MgTaO_6$ suggests the presence of 1/6 ($\sim 17\%$) of vacancies in the A-site position. Although neither neutron nor X-ray diffractions revealed a vacancy ordering, a short-range ordering cannot be excluded like it has been observed by Levin et al. [16] in $La_{1-x/3}[Mg_{(1-x)/2}Ti_{(1+x)/2}]O_3$ ($0.4 \leqslant x \leqslant 0.5$) and by Battle et al. [17] in $Sr_{1-3x/2}La_xTiO_3$ ($0.4 \leqslant x \leqslant 0.6$). To make a local probe of the crystal structure, electron diffraction experiments were performed in some grains and, indeed, a weak superstructure was found (Fig. 4). The $\langle 100 \rangle$ zone axes (Fig. 4a, b) clearly demonstrate that two of the three $\langle 100 \rangle$ pseudocubic translations are doubled. A doubling in the [110] direction is also clearly seen in the $\langle 111 \rangle$ zone axes patterns (Fig. 4c). This observation is consistent with

Table 2
Atomic coordinates and thermal parameters (B) for $La_{5/3}MgTaO_6$ at room temperature

Atom	Position	Occupation	x	y	z	B (Å²)
La	4i	0.83333	0.5026(18)	0	0.2533(26)	1.14
Mg	2a	1	0	0	0	0.12(5)
Ta	2d	1	0.5	0.5	0	0.78(5)
O1	4i	1	0.0705(11)	0	0.2528(28)	1.39
O2	8j	1	0.2592(36)	0.2561(36)	−0.0362(5)	2.49
	B_{11}(Å²)	B_{22}(Å²)	B_{33}(Å²)	B_{12}(Å²)	B_{13}(Å²)	B_{23}(Å²)
La	0.009(3)	0.011(2)	0.003(1)	0.00	0.005(3)	0.00
O1	0.003(2)	0.0020(2)	0.005(1)	0.00	0.004(3)	0.00
O2	0.032(4)	0.014(3)	0.008(1)	−0.002(2)	0.003(3)	0.001(3)

Space group $I2/m$; cell parameters: $a = 5.6304(2)$ Å, $b = 5.6226(2)$ Å, $c = 7.9434(2)$ Å, $\beta = 90.04(1)°$, $V = 251.47(2)$ Å³; $Z = 2$; calculated density of 7.64 g/cm³. Reliability factors: $R_p = 5.12\%$, $R_{wp} = 6.81\%$, $R_{Bragg} = 2.63\%$, $\chi^2 = 1.99$.

Table 3
Bond distances, angles and valence sums (BVS) for $La_{5/3}MgTaO_6$

Bond/bond angle	Multiplicity	Bond distance (Å)/angle (°)	Average bond distance (Å)	BVS
La–O1	×1	2.433(10)	2.788(7)	2.45(4)
La–O1	×2	2.842(2)		
La–O2	×2	3.039(19)		
La–O2	×2	2.617(19)		
La–O2	×2	2.600(18)		
La–O2	×2	3.018(19)		
Mg–O1	×2	2.047(22)	2.062(7)	2.21(4)
Mg–O2	×4	2.070(14)		
Ta–O1	×2	2.004(22)	1.968(7)	5.28(10)
Ta–O2	×4	1.950(14)		
O1				1.87(5)
O2				1.96(4)
Mg–O1–Ta		157.4(9)		
Mg–O2–Ta		163.5(6)		

the vacancy ordering type shown in Fig. 5(a). This means that the crystal structure of $La_{5/3}MgTaO_6$ in a short-range scale involves the interchange of the lanthanum rich and the lanthanum poor layers in both the [100] and [010] directions. This phenomenon is well known in $La_{2/3}TiO_3$, another A-site deficient perovskite [18], where the fully occupied (001) planes interchange with the 1/3-occupied ones resulting in a $a_p \times a_p \times 2a_p$ type superstructure. However, in contrast to $La_{2/3}TiO_3$, the vacancy ordering in $La_{5/3}MgTaO_6$ doubles in two pseudocubic directions. This type of vacancy ordering leads to the $P4/mmm$ space group, with a $2a_p \times 2a_p \times a_p$ unit cell. The simultaneous presence of the vacancy and the rock-salt type ordering in the A- and B-site positions, respectively, accounts for the $P4_2/mcm$ space group with the $2a_p \times 2a_p \times 2a_p$ unit cell. Simulations of the zone axes diffraction patterns give a good agreement with the electron diffraction experiment.

The doubling of two pseudocubic translations in Fig. 4b can be also a result of 90° domains, each with ordering in one direction only. However, this situation cannot take into account the {hk0; h, k = 2n+1} reflections which are coupled with the {hk0; h, = 2n+1, k = 2n} ones and appear always simultaneously. Besides, another interpretation of the observed superstructure can be done based on the assumption of a local in-phase tilting. In this case, symmetry of $La_{5/3}MgTaO_6$ in a short-range scale is monoclinic $P2_1/n$ and reflections of the {hk0; h, = 2n+1, k = 2n} type can be attributed to antiparallel A-site cation displacements. However, we suggest that this scenario is less probable because the sets of the {hk0; h, k = 2n+1} and {hk0; h, = 2n+1, k = 2n} reflections are decoupled in this case. Therefore, the pattern in Fig. 4b is a result of diffraction from three different domains and their relative intensity should strongly depend on grains. We examined numerous microcrystals and observed quite often ⟨100⟩

orientations with the $\{hk0; h, = 2n+1, k = 2n\}$ reflections (both single and multidomain), but the $\{hk0; h, k = 2n+1\}$ reflections never appeared without the $\{hk0; h, = 2n+1, k = 2n\}$ reflections doubling both the [100] and [010] pseudocubic translations.

At this stage the analogy with the crystal structures reported recently for the $La_4Mg_3W_3O_{18}$ [10] and $La_6Mg_4Ta_2W_2O_{24}$ [11] perovskites can be drawn. Besides the B-site cation ordering in these compounds there is also interchange between lanthanum rich, [LaO], and lanthanum poor [$La_{1/2}O$] layers, with the additional ordering vacancies
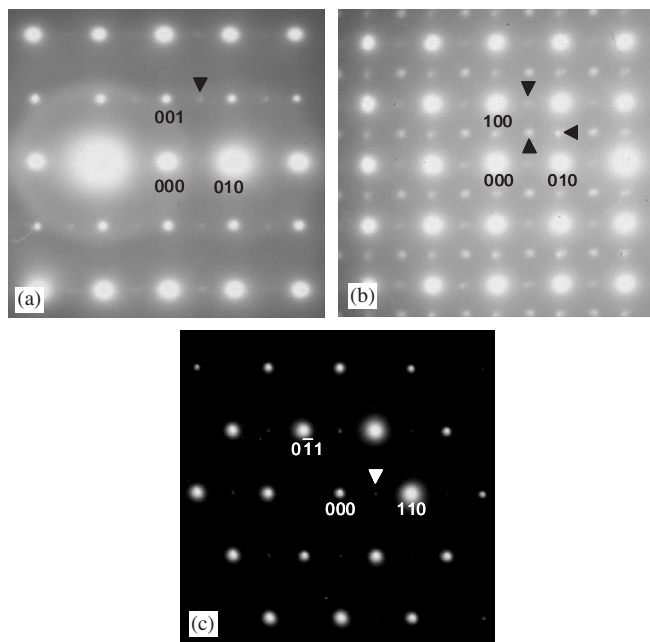

Fig. 4. Electron diffraction patterns obtained from $La_{5/3}MgTaO_6$ with zone axes chosen as [100] (a); [001] (b); and [111] (c).

into rows within the lanthanum poor layers (Fig. 5b and c). A half-period shift between [$La_{1/2}O$] layers gives rise to the superstructure of the $2a_p \times 4na_p \times 2a_p$ type, where $La_4Mg_3W_3O_{18}$ and $La_6Mg_4Ta_2W_2O_{24}$ are representatives of the $n = 1$ and 2 families, respectively. Based on the superstructure observed in these materials, a new homologous series, $A_{3n}B'_{2n}B''_{2n}O_{12n}$, was proposed. One can see from Fig. 5 that the distribution of the vacancies in the $La_{5/3}MgTaO_6$ perovskite in a short-range scale corresponds to the $n = \infty$ member of the series. This means that the half-period shift between the lanthanum poor layers is absent in this perovskite.

In Refs. [10,11] it was pointed that the half-period shift appears to avoid a cooperative character of the local distortions (lozenges in Fig. 5) originated from the different displacements of the B' and B'' cations. The local distortions are larger the greater the difference in the charge and size between the B' and B'' cations and the higher the concentration of the vacancies in the lanthanum poor layers. Due to a smaller amount of A-site vacancies in the case of $La_{5/3}MgTaO_6$, their distribution is rather random, and the difference in their concentration between lanthanum poor and lanthanum rich layers is small. This reduces strongly the driving force for the B-site cations displacements. As a result the local distortions in $La_{5/3}MgTaO_6$ are too weak to produce the half-period shift. However, the presence of random displacements of lanthanum and tantalum can be concluded from the high values of the isotropic thermal parameters obtained for these cations in the refinement of both the neutron ($B_{iso}(La) = 1.14 \,\text{Å}^2$, $B_{iso}(Ta) = 0.78 \,\text{Å}^2$) and X-ray ($B_{iso}(La) = 1.05 \,\text{Å}^2$, $B_{iso}(Ta) = 0.81 \,\text{Å}^2$) diffraction spectra.

To describe the symmetry of the crystal structure of $La_{5/3}MgTaO_6$ in a local level, both the vacancy ordering and the octahedral tilting must be taken into account.
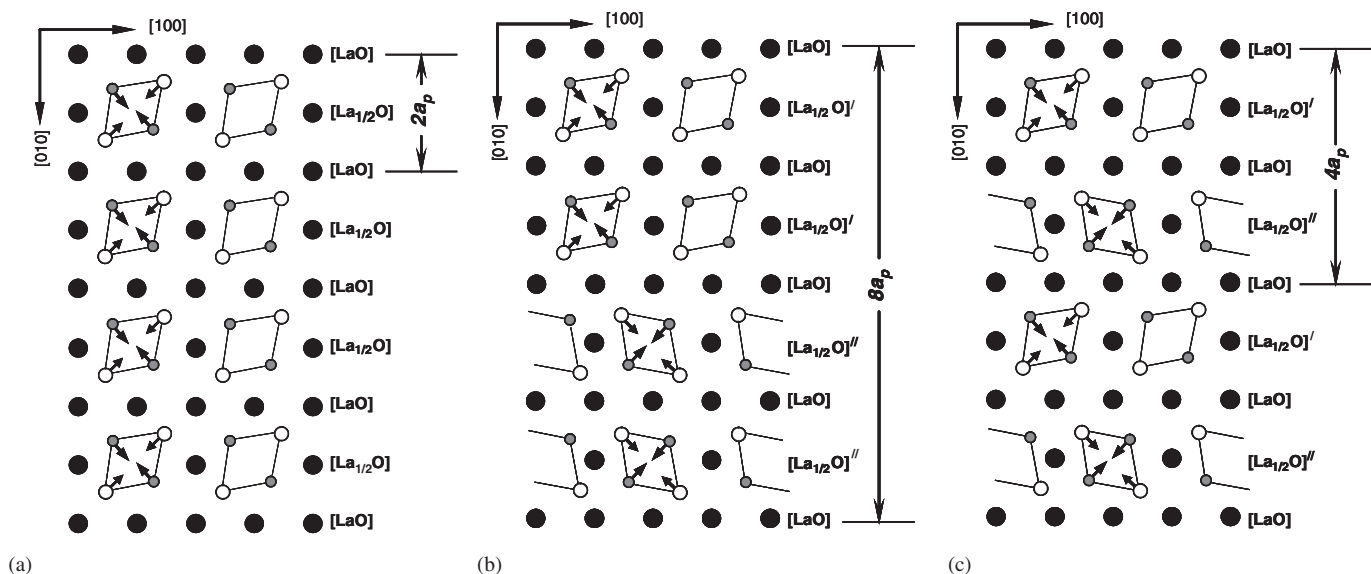

Fig. 5. Schematic representation of the A-site vacancy ordering in $La_{5/3}MgTaO_6$ (a), $La_6Mg_4W_2Ta_2O_{24}$ (b) and $La_4Mg_3W_3O_{18}$ (c). The local distortions are represented by lozenges.

According to the neutron diffraction data the octahedral tilting can be presented by the $a^- a^- c^0$ configuration. From the symmetry point of view, the most probable situation is when the octahedra rotate about the a- and b-axis of the $P4_2/mcm$ space group. This conclusion comes from the symmetry analysis of the possible tilt configurations in the $P4_2/mcm$ parent crystal structure. The analysis was done with the aid of the ISOTROPY software developed by Stokes and Hatch [19]. For the calculation the matrix of the Γ_4^+ and X_3^- irreducible representations of the $Fm\bar{3}m$ space group were used. These representations are associated with the A-site vacancy ordering and an antiphase octahedral tilting about $\langle 100 \rangle$ axes of the $Fm\bar{3}m$, respectively. The $\Gamma_4^+ \oplus X_3^-$ combination results in the four possible tilt configurations: $a^0 a^0 c^-$, $a^- b^0 c^0$, $a^- a^- c^0$ and $a^- b^- c^-$, with $P4_2/m$ ($2a_p \times 2a_p \times 2a_p$), $P2/c$ ($2a_p \times 2a_p \times 2a_p$), $C2/m$ ($2\sqrt{2}a_p \times 2\sqrt{2}a_p \times 2a_p$) and $P\bar{1}$ ($2a_p \times 2a_p \times 2a_p$) isotropy subgroups, respectively. Since the $a^- a^- c^0$ tilt system was found in the neutron diffraction experiment, the $C2/m$ space group is the most appropriate one for the description of the local crystal structure symmetry. A polyhedral representation of the structure is shown in Fig. 6. The difference in the symmetry between the ordered and the disordered crystal structures is in the unit cell dimension (in the translational symmetry). Attempts to refine the neutron and X-ray diffraction spectra in the ordered model allowing B-site cation displacements did not improve the refinement. Therefore the disordered structure can be considered as a good approximation for the crystal structure of $La_{5/3}MgTaO_6$ in a long-range scale.

3.2. Dielectric properties

Room temperature dielectric measurements at radio frequencies give a relative dielectric permittivity of $\varepsilon' \sim 23$. The permittivity increases linearly with temperature in the range of 290–500 K (Fig. 7 insert). Above 500 K a non-linear behaviour with a strong frequency dispersion is observed (Fig. 7). The temperature coefficient of the permittivity, $TC\varepsilon' = (1/\varepsilon')(\partial \varepsilon' / \partial T)$, evaluated from the linear part of $\varepsilon'(T)$, is 142 ppm K^{-1}. This value is typical
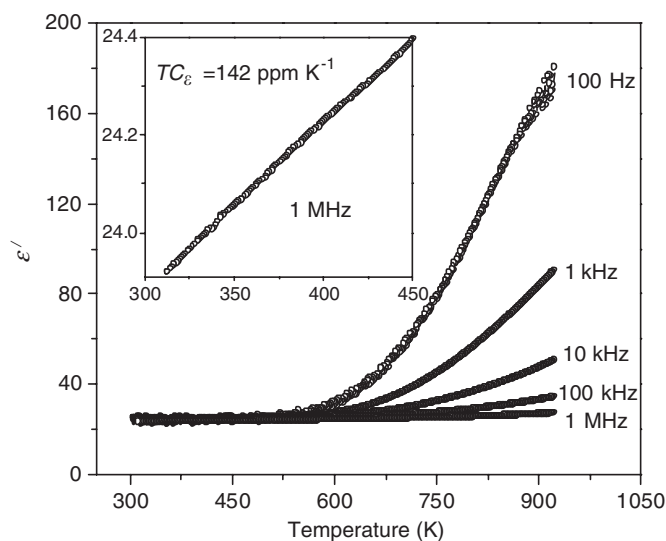
Fig. 7. Variation of the real part of the permittivity, measured at radio frequencies, with temperature.

for non-ferroelectric tilted perovskites in the vicinity of room temperature, where phonon contribution to ε' is predominant [20].

The room temperature permittivity measured by the resonant method at microwave frequencies ($f = 7.2$ GHz) is $\varepsilon' \sim 22.5$. This value agrees with that obtained at 1 MHz, which means that there is not any dispersion mechanism at the intermediate frequencies. It allows one to estimate the temperature coefficient of the resonant frequency, $TCf = -TC\varepsilon'2 - \alpha_l$ (α_l is the linear thermal expansion coefficient). Using the data on $TC\varepsilon'$ obtained at radio frequencies and taking $\alpha_l = 10$ ppm K^{-1} (a typical value for perovskite oxides), one obtains $TCf \sim -80$ ppm K^{-1}. This value is far from the technologically important criterion, $TCf \sim 0$, and indicates that in respect to microwave applications, the material can only be used in solid solutions with other compounds having a positive TCf coefficient.

Parameters of the resonant line yield the value of $Qf \sim 5000$ GHz. This value is unexpectedly low if one takes into account the perfect B-site cation ordering, which usually promotes a high value of the quality factor [21]. Microwave losses in ceramics are known to be caused by both extrinsic (porosity, impurities, grain boundaries, etc.) and intrinsic (lattice absorption due to crystal anharmonicity) factors. The extrinsic contribution can be minimized using proper processing conditions. Information on lattice anharmonicity in terms of the crystal structure symmetry can be drawn from FIR reflectivity spectra. Therefore, to evaluate the intrinsic (phonon) contribution to the dielectric function of $La_{5/3}MgTaO_6$, FIR spectroscopy was applied.

The FIR reflectivity spectrum is shown in Fig. 8. The data were fitted with the factorized form of the dielectric function assuming six active modes. This number of modes was preliminary determined based on the ε'' spectrum
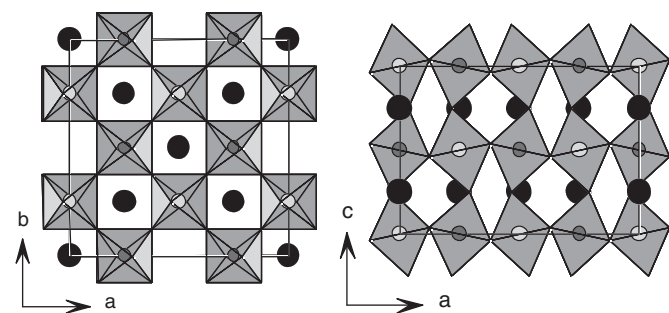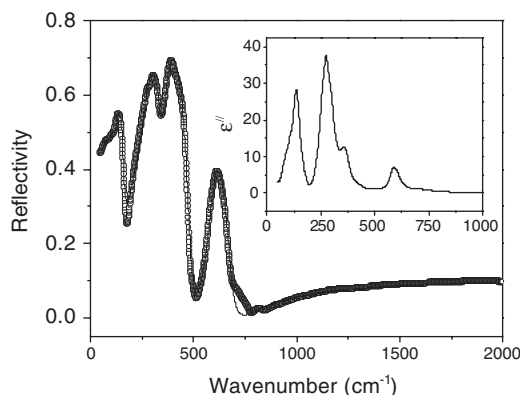

Fig. 6. Polyhedral representation of the crystal structure of $La_{5/3}MgTaO_6$ involving the short-range A-site vacancy ordering ($C2/m$ symmetry, $2\sqrt{2}a_p \times 2\sqrt{2}a_p \times 2a_p$ unit cell).

Fig. 8. FIR reflectivity spectrum of $La_{5/3}MgTaO_6$: experimental data (open symbols) and fitting (solid line). The insert shows the imaginary part of the dielectric function obtained by the Kramers–Kronig inversion.

obtained by the Kramers-Kroning inversion (Fig. 8 inset). Considering the disordered model of the crystal structure obtained from the neutron diffraction experiment, the following decomposition of the normal modes at the Γ point is expected based on the factor group analysis [22]: $7A_g + 7A_u + 5B_g + 11B_u$. The infrared active representations are $6A_u + 9B_u$. The lower number of the experimentally observed modes in comparison with this symmetry prediction is not unexpected, because in the case of ceramic samples the anisotropy may be averaged out. Therefore, A_u and B_u modes may not be entirely resolved. Moreover, the bands related to the displacements of the oxygen atoms are often too weak to be detected or overlap with other intense bands.

In order to evaluate the contribution of the polar lattice phonons to the dielectric response measured at microwave frequency range, we evaluated the real (ε') and the imaginary (ε'') parts of the IR dielectric function at $0.26\,cm^{-1}$ (7.8 GHz). We obtained the values $\varepsilon' = 23$ and $\varepsilon'' = 8.4 \times 10^{-3}$. Thus, the magnitude of Qf at microwave range evaluated from the infrared spectroscopy data is $\sim21000\,GHz$. This indicates that even the lowest limit of the intrinsic dielectric loss in $La_{5/3}MgTaO_6$ is very high in comparison with other ordered stoichiometric perovskites like, for example, La_2MgTiO_6 or Ba_2InTaO_6, where Qf is $114\,000\,GHz$ [23] and $130\,000\,GHz$ [24], respectively. Since the refinement of the X-ray diffraction data revealed that $La_{5/3}MgTaO_6$ exhibits a very high degree of B-site ordering, it seems reasonable to correlate the higher intrinsic losses to the high concentration of A-site vacancies. The mechanism of dielectric losses connected with the presence of vacancies can be understood on the base of a "spatial correlation" model discussed in Ref. [2]. In this model, the vacancies break the local symmetry and shorten the phonon coherence length. The finiteness of the phonon correlation is accounted for by introducing a spatial correlation function. In the "ideal" crystal lattice (in respect to translational symmetry) the spatial correlation function is infinity. In real crystals, it depends on the

concentration of defects. This results in a breakdown of the $k = 0$ selection rule and an increase of multiphonon absorption, which is the dominant mechanism of dielectric loss in the microwave frequency range [25,26].

4. Conclusions

The crystal structure of the A-site deficient $La_{5/3}MgTaO_6$ perovskite in a long-range scale is characterized by the monoclinic $I2/m$ space group, with the following parameters of the unit cell: $a = 5.6304(2)\,\text{Å}$, $b = 5.6226(2)\,\text{Å}$, $c = 7.9434(2)\,\text{Å}$ and $\beta = 90.04(1)°$. The structural model involves rock-salt type ordering between Mg^{2+} and Ta^{5+} cations and an antiphase octahedral tilting, with the $a^- a^- c^0$ configuration. In a short-range scale the A-site vacancy ordering exists. The ordering results in the interchange of lanthanum rich and lanthanum poor layers in both the [100] and [010] directions. The crystal structure symmetry at the local level can be described by the $C2/m$ space group with the $2\sqrt{2}a_p \times 2\sqrt{2}a_p \times 2a_p$ supercell.

The static dielectric permittivity of $La_{5/3}MgTaO_6$ at room temperature is ~23 and increases with temperature. The values of the permittivity measured in the microwave and radio frequencies ranges were found to agree with the one extrapolated from the FIR data. The thermal coefficient of the permittivity estimated from the temperature dependence of the dielectric permittivity measured at $1\,MHz$ is $142\,ppm\,K^{-1}$, which is a typical value for non-ferroelectric tilted perovskites. The complex dielectric function extrapolated from FIR data down to the gigahertz range allowed to estimate the phonon contribution to the dielectric loss. The estimated value indicates a considerable intrinsic loss in $La_{5/3}MgTaO_6$. This behaviour can be explained by the reduction of the spatial phonon correlation due to the presence of the strongly disordered A-site vacancies. The finiteness of the phonon correlation results in the breakdown $k = 0$ selection rule and increases the probability of the multiphonon absorption at microwave frequencies.

References

[1] T.A. Vanderah, V.L. Miller, I. Levin, S.M. Bell, T. Negas, J. Solid State Chem. 177 (2004) 2023.
[2] A.N. Salak, D.D. Khalyavin, V.M. Ferreira, J.L. Ribeiro, L.G. Vieira, J. Appl. Phys. 99 (2006) 094104.

[3] Y. Inaguma, L.Q. Chen, M. Itoh, T. Nakamura, T. Uchida, H. Ikuta, M. Wakihara, Solid State Commun. 86 (1993) 689.

[4] A. Morata-Orrantia, S. Garcia-Martin, M.A. Alario-Franco, Chem. Mater. 15 (2003) 3991.

[5] S. Stramare, V. Thangadurai, W. Weppner, Chem. Mater. 15 (2003) 3974.

[6] G. Blatter, M.V. Feigelman, V.B. Geshkenbein, A.I. Larkin, V.M. Vinokur, Rev. Mod. Phys. 66 (1994) 1125.

[7] J.L. MacManus Driscoll, Adv. Mater. 9 (1997) 457.

[8] C. Martin, A. Maignan, D. Pelloquin, N. Nguyen, B. Raveau, Appl. Phys. Lett. 71 (1997) 1421.

[9] I.O. Troyanchuk, N.V. Kasper, D.D. Khalyavin, H. Szymczak, R. Szymczak, M. Baran, Phys. Rev. Lett. 80 (1998) 3380.

[10] D.D. Khalyavin, P.Q. Mantas, A.M.R. Senos, J. Phys.: Condens. Matter 17 (2005) 2585.

[11] D.D. Khalyavin, A.B. Lopes, P.Q. Mantas, A.M.R. Senos, Chem. Mater. 18 (2006) 3843.

[12] J. Rodriguez-Carvajal, Physica B 192 (1993) 55.

[13] B.W. Hakki, P.D. Coleman, IRE Trans. Microwave Theory Technol. 8 (1960) 402.

[14] Y. Kobayashi, M. Katoh, IEEE Trans. Microwave Theory Technol. 33 (1985) 586.

[15] C.J. Howard, B.J. Kennedy, P.M. Woodward, Acta Crystallogr. B 59 (2003) 463.

[16] I. Levin, T. Vanderah, T.G. Amos, J.E. Maslar, Chem. Mater. 17 (2005) 3273.

[17] P.D. Battle, J.E. Bennett, J. Sloan, R.J.D. Tilley, J.F. Vente, J. Solid State Chem. 149 (2000) 360.

[18] C.J. Howard, Z. Zhang, J. Phys.: Condens. Matter. 15 (2003) 4543.

[19] H. T. Stokes, D. M. Hatch, ISOTROPY, 2002. http://stokes.byu.edu/isotropy.html.

[20] I.M. Reaney, E.L. Colla, N. Setter, Jpn. J. Appl. Phys. 33 (1994) 3984.

[21] R.J. Cava, J. Mater. Chem. 11 (2001) 54.

[22] D.L. Rousseau, R.P. Bauman, S.P.S. Porto, J. Raman Spectrosc. 10 (1981) 253.

[23] M.P. Seabra, A.N. Salak, V.M. Ferreira, J.L. Ribeiro, L.G. Vieira, J. Eur. Ceram. Soc. 24 (2004) 2995.

[24] R. Zurmühlen, J. Petzelt, S. Kamba, G. Kozlov, A. Volkov, B. Gorshunov, D. Dube, A. Tagantsev, N. Setter, J. Appl. Phys. 77 (1995) 5351.

[25] M. Sparks, D.F. King, D.L. Mills, Phys. Rev. B 26 (1984) 6987.

[26] V.L. Gurevich, A.K. Tagantsev, Adv. Phys. 40 (1991) 719.